THE JOURNAL OF PHYSICAL CHEMISTRY C
A JOURNAL OF THE AMERICAN CHEMICAL SOCIETY

pubs.acs.org/JPCC
Article

Nonorthogonal Configuration Interaction for Singlet Fission: Beyond the Dimer

Published as part of The Journal of Physical Chemistry C special issue "Francesc Illas and Gianfranco Pacchioni Festschrift".

C. Sousa,* X. López, X. Dong, R. Broer, T. P. Straatsma, and C. de Graaf

Cite This: J. Phys. Chem. C 2025, 129, 4290−4302

ABSTRACT: Non-orthogonal configuration interaction with fragment calculations are presented for a number of compounds that show singlet fission properties: (i) four perylene-diimide derivatives, (ii) crystalline pentacene and its (B,N)-substituted variant, and (iii) a regular and a distorted stack of three indolonaphthyridine molecules. The electronic couplings between the singlet excitonic states (S_1) and the singlet-coupled double triplet (T_1T_1), the so-called singlet fission coupling, were computed from ensembles with two and three molecules, and except for some small deviations when charge transfer states were included, results are virtually the same. Ensembles of three molecules were used to study the mechanisms of triplet separation, double triplet diffusion, and singlet and triplet exciton diffusion. The calculations show that apart from the standard mechanism for the generation of two uncoupled triplet states ($S_1 \rightarrow T_1T_1 \rightarrow T_1...T_1$), there are two other possible pathways: the direct generation from the singlet excitonic state ($S_1 \rightarrow T_1...T_1$) and the process in which the excitonic state evolves in a superposition of T_1T_1 and $T_1...T_1$ states. The electronic coupling for triplet diffusion is in general much smaller than for singlet diffusion.

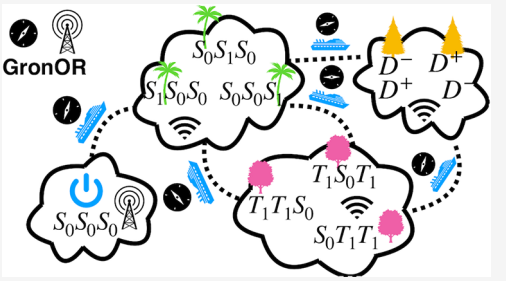

1. INTRODUCTION

Multiple exciton generation may increase significantly the efficiency of (organic) solar cells. Instead of converting an incoming photon into a single exciton, i.e., a single bound electron−hole pair, the absorption process excites multiple electrons from the valence to the conduction band (or from high lying occupied orbitals to low lying unoccupied orbitals in the case of molecular crystals). There are several candidate mechanisms for the formation of more than one exciton and one of them, singlet fission, occurs through intermolecular energy transfer. This singlet fission process is generally conceptualized as occurring in two consecutive steps. First, a local excited singlet state (S_1) transfers approximately half of its excess energy to a neighboring unit, and by falling back to a lower lying local triplet state (T_1) a similar triplet state on the neighbor is created. The spin moments of the two triplets are coupled to an overall singlet state, making it a spin-allowed process. In the second stage, this entangled double triplet state (T_1T_1) separates into two independent triplets.

$$S_1S_0 \rightarrow T_1T_1 \rightarrow T_1...T_1 \quad (1)$$

Theoretical studies of intermolecular singlet fission with ab initio methods have been mostly focused on monomers or ensembles with two molecules. Isolated molecules have been used to find (new) compounds for which the energy difference between the ground state (S_0) and the lowest triplet state (T_1) is approximately half the energy difference between S_0 and S_1, the lowest singlet state. In this way, several interesting candidates for singlet fission have been identified[1−4] and additional understanding has been developed of the factors that govern this energy difference. There appears to be a trade-off between a certain amount of biradical character to obtain a low-lying triplet state and chemical stability, favored by a large HOMO−LUMO gap.[5−8]

The inclusion of a second molecule in the material model opens the possibility to study some of the fundamental mechanisms of singlet fission such as the conversion of a singlet excitonic state (S_1) into a singlet-coupled double triplet (T_1T_1). The role of the charge-transfer (CT) states has been at the center of attention in many studies and three different pathways connecting S_1 and T_1T_1 have emerged,[9] whose relative importance depends on the particularities of each compound. In the mechanism that directly couples the two

Received: December 23, 2024
Revised: February 5, 2025
Accepted: February 10, 2025
Published: February 17, 2025

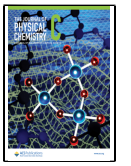

https://doi.org/10.1021/acs.jpcc.4c08656
J. Phys. Chem. C 2025, 129, 4290−4302

states, the role of the CT states is negligible (for example, in systems where these states lie high in energy). In a second mechanism, the CT states are considered to be intermediate states in a two-step process, which requires them to be energetically very close to the S_1 and T_1T_1 states. Third, the so-called CT-enhanced mechanism is a one-step process in which the S_1 and/or T_1T_1 states have significant CT character, which increases the electronic coupling of initial and final states. If the CT character of the S_1 state is important, a model containing at least all nearest neighbors of a central molecule is preferable. In case of stacks of molecules this leads to a three molecule ensemble.

The relation between the relative orientation of the molecules and the electronic coupling of the singlet exciton with the double triplet, known as the *singlet fission coupling*, can also be addressed with dimer ensembles and several studies have explored the conformational space to establish which geometrical parameters govern this coupling[10,11] with the aim to formulate design rules for new materials with improved singlet fission properties.

Clearly, the dimer models can only describe part of the singlet fission process. After the formation of the singlet-coupled double triplet, the entangled T_1T_1 must dissociate and diffuse as independent triplet excitons.[12−14] Subsequently, the hole and particle pair should convert into two separate charge carriers. In nanostructured materials, it is usually assumed that charge separation occurs at interfaces between nano structures. In molecular materials, the study of the dissociation of the T_1T_1 state into a $T_1...T_1$ state requires an ensemble of at least three molecules.[15] Experimental evidence for the existence of the T_1T_1 state as intermediate in the generation of multiple separated excitons through singlet fission was published by Yong and co-workers.[16] They established a binding energy of the two triplets of approximately 30 meV in a family of pentacene and tetracene derivatives and discussed several pathways along which this state can evolve. It either separates into two independent triplet excitons, falls back to the S_0 (through nonradiative processes or by photoluminescence), or recombines to the S_1 state. In a follow-up paper by Bossanyi et al.[17] these findings were put on a more firm basis and direct evidence for the T_1T_1 state in pentacene was presented. T_1T_1 states were also observed within covalently linked indolonaphthyridine units, but the rapid deactivation to the ground state makes these molecular constructs less suitable for singlet fission.[18] In a comparison of the singlet fission efficiency of four perylenediimide (PDI) derivatives, a delicate balance was observed between a fast singlet fission rate (formation of the T_1T_1 state and subsequent triplet separation) and the recombination of these two triplets. Those conformations that show fast triplet formation are also the ones for which the highest decay rates were observed.[19]

The extension of the model to three units also enables the study of alternative scenarios for the formation of the $T_1...T_1$ state, namely directly from the S_1 state without an intermediate T_1T_1 state. The transition from S_1 to $T_1...T_1$ is highly unlikely in a direct fashion, but the coupling between the singlet exciton and the dissociated double triplet could become sizable when CT configurations are taken into account. Wang and co-workers distinguished two processes for the evolution of the singlet excitonic state in an experimental study on covalently linked tetracenes[20]; a fast process in which the singlet coupled double triplet is formed and a much slower process in which the $T_1...T_1$ state is directly formed without intermediate T_1T_1 states. The latter process was argued to be only possible in certain thermally distorted conformations for which the so-called long-range charge transfer states (with the hole and electron localized on non-neighboring units) are significantly lowered in energy.

The three-molecule ensemble also gives a first impression of the degree of delocalization of the excitonic states and to what extent this affects their energy. The bandwidth of the singlet excitonic band in acenes has been estimated to be on the order of 100 meV, the triplet exciton band was assigned a width of 50 meV[21] and the T_1T_1 bandwidth was hypothesized to lie in between these two values.[12] Obviously, larger ensembles are required to get a full picture,[22] but this goes beyond the scope of our present study.

Here we study three different materials that show singlet fission. In the first place, four perylene diimide (PDI) derivatives are selected from those that were studied in ref 23. Second, we focus attention on pentacene and a B,N-substituted variant, which has been mentioned in several studies as interesting alternative for the parent compound.[5,24−26] The dimers of these two compounds have already been studied in our group, and hence, a detailed comparison between dimer and trimer results can be made. The third compound that has been studied is indolonaphthyridine. Here, we compare a regular stack of three molecules with a thermally distorted stack extracted from a molecular dynamics simulation of a ten-membered stack.

The remainder of the paper is organized as follows: After a short description of the Non-Orthogonal Configuration Interaction approach applied here to calculate the relevant electronic couplings in Section 2, the singlet fission chromophores are presented (Section 3). Next, the computational information employed to evaluate the energies and electronic couplings of the materials studied is listed in Section 4. The results section is divided into three parts, each dealing with a specific kind of intermolecular energy transfer process. Section 5.1 compares the singlet fission couplings in dimers and trimers to establish the transferability of the calculated couplings. Section 5.2 exposes the results on the triplet separation and double triplet diffusion. The last part of the results (Section 5.3) describes the singlet and triplet exciton diffusion in the three compounds and discusses the implications of the higher or lower mobility for the singlet fission process. The paper ends with a short summary of the most important findings of this study.

2. NON-ORTHOGONAL CONFIGURATION INTERACTION FOR FRAGMENTS

As a continuation of our ab initio studies of the first stages of the singlet fission process in dimers,[23,26,27] we present here the results of a series of Non-Orthogonal Configuration Interaction with Fragments (NOCI-F) calculations applied to ensembles with three molecules focusing on the process of triplet separation (formation of the $T_1...T_1$ state) and the diffusion of both the singlet and triplet exciton through the material. NOCI-F is a versatile computational strategy to obtain information about the couplings among the electronic states involved in the intermolecular energy and electron transfer processes. The procedure starts with the separate optimization of a multiconfigurational wave function for a collection of electronic states on the different molecules (fragments) in the ensemble, namely the ground state (S_0), a local excited singlet (S_1) and triplet state (T_1), plus the cationic

https://doi.org/10.1021/acs.jpcc.4c08656
J. Phys. Chem. C 2025, 129, 4290−4302

and anionic doublets (D^+ and D^-). The individual optimization of the wave function ensures that all states are expressed in their own optimal orbital set, which is specially relevant for the D^+ and D^- states as orbital relaxation with respect to the ground state orbitals is large for these states.

The next step is to construct the electronic states of the complete ensemble. This is done by combining the fragment states into spin-adapated antisymmetrized products. For example, taking the ground state function of fragment A, the cationic state of B and the anionic state of C, a multiconfigurational wave function can be created for the trimer ensemble ($S_{0,A}D^+_BD^-_C$) that represents a pure charge transfer state and whose orbitals are optimally adapted to this electronic configuration. The trimers result in a total of 13 relevant ensemble electronic states with singlet spin moment: the overall ground state ($S_0S_0S_0$), three local excited singlets ($S_1S_0S_0$, $S_0S_1S_0$, $S_0S_0S_1$), two coupled triplets ($T_1T_1S_0$, $S_0T_1T_1$), the $T_1...T_1$ state ($T_1S_0T_1$) and six charge transfer states ($D^+D^-S_0$, $D^-D^+S_0$, $S_0D^+D^-$, $S_0D^-D^+$, $D^+S_0D^-$, $D^-S_0D^+$), where the last two are the states hypothesized by Wang et al.[20] to be responsible for enabling the formation of the $T_1...T_1$ directly from the S_1 without passing through the T_1T_1 state. In the case of a two-molecule ensemble, or dimer, the list of states reduces to six: S_0S_0, S_1S_0, S_0S_1, T_1T_1, D^+D^- and D^-D^+.

These singlet spin states are the nonorthogonal many-electron basis functions (MEBFs) for the NOCI-F calculation. The Hamiltonian and overlap matrix elements can be used to calculate the electronic coupling between the diabatic states (cf. eq 2)

$$\gamma_{ij} = \frac{H_{ij} - \frac{1}{2}(H_{ii} + H_{jj})S_{ij}}{1 - S_{ij}^2} \tag{2}$$

or one can solve the general eigenvalue problem to obtain the adiabatic representation of the many-electron states of the ensemble and their corresponding energy eigenvalues. This NOCI-F approach to study the electronic structure of ensembles of molecules relevant to singlet fission has several advantages. The description includes both the static and dynamic electron correlation effects,[27] it contains full orbital relaxation, but still the final many-electron wave functions are expressed in a limited number of clearly identifiable diabatic states, which makes the interpretation of the results straightforward. This combination of accuracy and maintaining the simplicity of (empirical) models is not easily found in standard quantum chemical approaches based on orthogonal orbitals. The price to pay is the higher computational complexity of the approach. Each matrix element of the NOCI-F Hamiltonian is the sum of the contributions of thousands of determinant pairs from both the *bra* and *ket* functions and the calculation of each of these contributions is significantly more complex than in the case of orthogonal determinants. On the other hand, NOCI-F has been implemented in the massively parallel and GPU accelerated computer code GronOR.[28,29] Combined with the application of a reduced common molecular orbital basis,[30] the method can be used to study in great detail ensembles as large as trimers of molecules that are relevant to singlet fission. More information on the NOCI-F approach and technical details of the computation of the matrix elements and the construction of the reduced common molecular orbital basis can be found in refs 28−32.

To distinguish between the above-described mechanisms for singlet fission, we not only determine the direct coupling between the S_1S_0 and T_1T_1 states by applying eq 2, but also calculate the effect of the charge transfer configurations on this coupling. For this purpose a new set of MEBFs is constructed through partial diagonalizations of the NOCI-F matrix. On the one hand, these partial diagonalizations involve the singlet exciton and CT states and on the other hand, the double triplet and CT states. The eigenvectors of the partial diagonalizations with the largest weight on the singlet excitonic and double triplet states define the new set of CT dressed MEBFs for which the coupling is calculated by applying eq 2. Furthermore, the coupling is corrected for the energy effect of dynamic correlation as outlined in ref 27. This resulting coupling is referred to as total coupling in the discussion of the results. The effect of CT configurations and dynamic correlation was not only included in the singlet fission coupling, but also in the other electronic couplings discussed in this study.

3. SINGLET FISSION CHROMOPHORES

Figure 1 depicts the basic structure of the three singlet fission chromophores of this study. On the left, there is the perylene

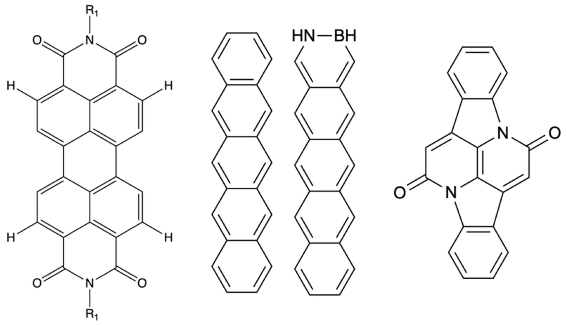

Figure 1. Basic structures of the singlet chromophores. Left: Perylenediimide, middle: Pentacene and B,N-pentacene, right: Indolonaphthyridine.

diimide skeleton. The relative orientation of the PDI molecules depends on the nature of the R_1-group. The four different geometries studied are extracted from the crystal structures of PDI derivatives with R_1 = ethylphenyl (EP), propyl (C3−I), heptyl (C7) and octyl (C8). In all cases the molecules are parallel to each other but the displacements along x, y and z are different (see ESI, Table S1 and Figure S1). Replacing the R_1-group by hydrogen has little influence on the relative energies of the fragment states,[33] but R_1 can affect the electronic couplings in some cases.[23]

Crystalline pentacene is a widely studied material for its singlet fission properties. Based on the heteroatom substitution strategy proposed by Zeng et al.,[5] there have been several (theoretical) studies in which two carbon atoms were replaced by a B−N pair.[34−36] The B,N-pentacene shown in the middle panel of Figure 1 was demonstrated in a previous study to be among the most stable substituted derivatives and to have a triplet excitation energy that is half the energy of the first excited singlet.[26]

Pentacene crystallizes in the so-called herringbone structure as illustrated in Figure 2. The unit cell has two symmetry unique molecules (A and B in the figure) giving rise to nearest and next nearest neighbor interactions of different nature.

https://doi.org/10.1021/acs.jpcc.4c08656
J. Phys. Chem. C 2025, 129, 4290−4302

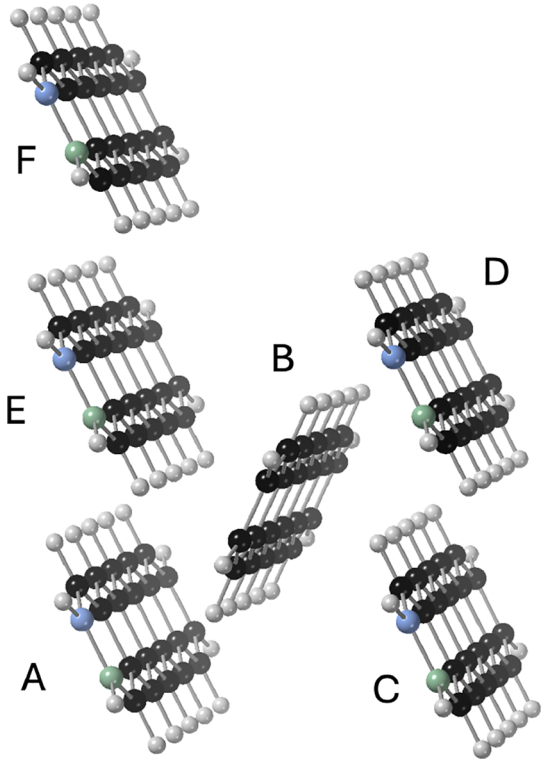

Figure 2. Crystal packing used for the B,N-pentacene system. Units A, C−F are B,N-pentacene molecules, unit B represents an unsubstituted pentacene. The pure pentacene model presents the same packing. Black spheres represent carbon atoms, light blue is nitrogen, green is boron and white is hydrogen.

Parallel aligned molecules (A−E, A−C, etc.) are expected to show weak singlet fission couplings, but rather strong exciton transfer. For the nonparallel molecules (A−B, B−C, etc.), the opposite is expected.[37,38]

Indolonaphthyridine has been proposed as singlet fission chromophore by Fallon and co-workers based on the special excited state aromatic properties because of the presence of a $[4n]$ five-membered ring next to a $[4n + 2]$ six-membered ring.[4,7] Figure 3 shows the two stacks that are compared. In the regular stack, shown on the left, the molecules are displaced with respect to each other by $\Delta x = 2.6$ Å, $\Delta y = 1.5$ Å, and $\Delta z = 3.5$ Å (with the long molecular axis along x). Taking the midpoint of the central C−C bond as reference point, the displacements (in Å) of the molecules in the distorted stack are (1.004, 1.719, 3.359) from A to B, and (−1.004, −1.719, 3.359) from B to C. The angle between the central C−C bonds of A and B is 33.7, and 8.2° for B and C.

4. COMPUTATIONAL INFORMATION

The ground state geometry of the PDI monomer has been optimized by Density Functional Theory (DFT) using the BP86-D3[39,40] hybrid functional and the D3 van der Waals dispersion energy correction by Grimme et al.[41] as done in a previous work.[23] Triple-ζ valence plus polarization Gaussian basis sets[42] (def2-TZVP) were applied for all atoms. These calculations were performed using the Orca 4.2.0 code.[43] The PDI optimized geometry for the S_0 ground state shows a planar D_{2h} symmetry, as shown in Figure 1. The dimers and trimers are constructed by applying a translation with Δx, Δy and Δz corresponding to the crystal structure of the four derivatives studied here.

The crystal structures of pentacene and B,N-pentacene have been optimized by periodic DFT calculations performed with the VASP 5.3.5 code.[44−47] Atomic positions as well as lattice parameters were allowed to relax and a Γ-centered $2 \times 2 \times 2$ k-point grid was employed for the Brillouin zone integration. The valence electrons were described using a plane wave basis set with a kinetic energy cutoff of 700 eV. The PBE-vdW[41,48] functional has been used and the convergence criteria for the self-consistent field energies and the structural relaxation were set to 10^{-7} eV. More details of the optimized structural parameters can be found in ref 26.

The geometry of the indolonaphthyridine molecule has been determined in two ways. The regular structure has been obtained by optimizing the molecule in vacuum at the DFT level with the NWChem program.[49] The B3LYP[50,51] hybrid functional has been applied and def2-TZVP[42] Gaussian basis sets were used for all atoms. Also, a thermally distorted model of stacked indolonaphtyridine units was obtained with classical molecular dynamics (MD) using the GROMACS 2019.3 version[52,53] and the AMBER99 force field.[54] A four-step simulation was performed, i.e., three preproduction calculations including energy minimization of the system, a 1 ns NVT run and a 1 ns NPT run, and a production NVT run of 50 ns. In the latter, the v-rescale algorithm,[55] an extension of the Berendsen thermostat to sample a canonical ensemble, was applied to simulate a $T = 300$ K bath. The model contains a solution of 10 randomly distributed indolonaphthyridine molecules in 1426 dimethylformamide molecules in a cubic box of dimensions $(5.7\ \text{nm})^3$ under periodic boundary conditions. During the simulation, the system evolves to a nine-membered indolonaphtyridine stack. From this arrangement, one trimer was selected from a snapshot along the MD trajectory to calculate the electronic couplings discussed above.

For all molecules, state specific Complete Active Space Self Consistent Field (CASSCF) and partially contracted N-Electron Valence State Second-Order Perturbation Theory (PC-NEVPT2)[56,57] calculations have been performed with

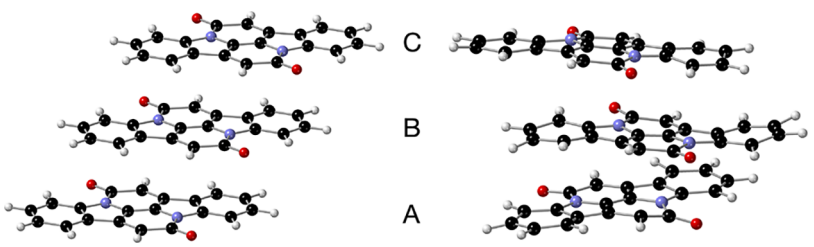

Figure 3. Regular (left) and thermally distorted (right) three-molecule stack of indolonaphthyridine. The molecules in both stacks are labeled from the bottom up as A, B, and C.

https://doi.org/10.1021/acs.jpcc.4c08656
J. Phys. Chem. C 2025, 129, 4290−4302

OpenMolcas.[58,59] ANO-RCC basis sets[60] with a (4s,3p,1d) contraction for second row elements and (3s,1p) for H were applied. All electrons were included in the perturbational treatment of the dynamic electron correlation except for the deep-core electrons, i.e., $1s^2$ for B, C, N and O. An active space containing 8 π orbitals and 8 electrons, CAS(8,8), has been considered to describe the two lowest singlets, S_0 and S_1, and the lowest-lying triplet, T_1, states, while the cationic D^+ state has one electron less in the active space, resulting in a CAS(7,8) and the anionic D^- one electron more, CAS(9,8). These fragment wave function were used to construct the MEBFs in the subsequent NOCI-F calculations, using the GronOR code[28,29] The MEBFs mainly account for non-dynamic molecular electron correlation. The energy contribution of the remaining, mainly dynamic, electron correlation is included by shifting the diagonal elements of the NOCI matrix by a second-order perturbation theory correlation energy correction on the MEBFs.[27] This correction is computed from the PC-NEVPT2 energy for each electronic state of the monomer. Hence, the total coupling as referred to in the discussion includes the effects of the CT states and the PC-NEVPT2 electron correlation correction.

5. RESULTS AND DISCUSSION

5.1. Singlet Fission Couplings: Dimers versus Trimers.

Upon the generation of a singlet excited state S_1 by the absorption of light, an intermolecular energy transfer from the excited molecule to a neighboring molecule in the ground state (S_0) may occur, resulting in the formation of two triplet states on neighboring molecules coupled to singlet spin, the T_1T_1 state. The feasibility of this first stage of the singlet fission process is related to the electronic coupling between the initial S_1S_0 state and the final T_1T_1 state.[61] In the dimer case, two couplings can be calculated: S_1S_0 or S_0S_1 with T_1T_1 in a localized picture of the singlet exciton. These two couplings are strictly identical (γ) when the dimer has an inversion center, but can be slightly different in conformations that break the inversion symmetry ($\gamma \pm \delta$). In a delocalized picture of the singlet exciton ($S_1S_0 \pm S_0S_1$), the coupling with T_1T_1 in a dimer with inversion symmetry is zero for the minus combination and $\sqrt{2}\gamma$ for the plus combination. Again, for dimers without inversion symmetry, the situation is slightly more complicated and both couplings are nonzero. A similar analysis can be made for trimers. There are four nonzero interactions in the localized description (γ) of the conformationally symmetric trimer, which converts to three nonzero interactions in the delocalized description ($\gamma, \frac{1}{2}\sqrt{2}\gamma \pm \gamma$). As for the dimer, these relations do not hold any longer in the absence of an inversion center.

The squared electronic couplings enter Fermi's golden rule for the rate of the transition. It can be seen that the sum of the squared couplings is exactly the same in the localized and delocalized pictures: $2\gamma^2$ in the dimer and $4\gamma^2$ in the trimer. To facilitate the comparison of the results of the two ensembles, we will report γ extracted from the sum of the squares of all interactions. A more detailed account on the relation between (de)localization and singlet fission couplings can be found in ref 22.

5.1.1. Perylene Diimide. In Table 1 the values of the coupling parameter γ are presented for the dimer and trimer models of the four PDI derivatives studied (Figure 4). Results show good agreement of the coupling values of the dimer and trimer models, both for the direct coupling (γ direct) and the CT enhanced and PC-NEVPT2 shifted coupling (γ total), implying that a dimer model is large enough to catch the magnitude of the SF coupling. Inclusion of charge transfer states and the effect of electron correlation on the SF process largely increases the value of the coupling, leading to values of γ total that are 1 order of magnitude larger than γ direct. Not unexpectedly, the dimer−trimer differences between γ total are larger than between γ direct, due to the more complete account of charge transfer in the trimers. The major role of charge transfer states in the SF process for PDI derivatives has been reported in a previous studies.[23,33]

Table 1. Direct and Total SF Electronic Couplings γ (in meV) for Dimers and Trimers of Various PDI Derivatives

	dimer		trimer	
	γ direct	γ total	γ direct	γ total
EP	2.24	25.68	2.28	27.60
C3−I	1.16	34.43	1.20	33.11
C7	4.14	33.47	4.13	30.68
C8	7.74	17.54	7.72	26.78

To further check the consistency of the results obtained for the ensembles in vacuum, a new model consisting of a dimer surrounded by two PDI units represented by a frozen density has been considered for the EP derivative (see Figure 4). In this embedded dimer model, the two outermost PDI molecules are described by the electronic density obtained in a Hartree−Fock calculation of the monomer ground state, S_0, applying a minimal basis set for all atoms. Results procure for the embedded dimer model almost match those obtained for the dimer representation, thus revealing the adequacy of the molecular ensembles in vacuum to study SF couplings. For the EP conformation, the embedded model gives a γ direct of 2.31 meV, to be compared with 2.24 meV for the dimer in vacuum, while the γ total value becomes 22.75 meV, very close to the coupling obtained by the bare dimer, 25.68 meV.

5.1.2. Pentacene and B,N-Pentacene. The results related to model crystals of pentacene and B,N-pentacene are shown in Tables 2 and 3, respectively. We observe that γ direct computed from dimer and trimer models of the same pair are practically the same, suggesting that this parameter is not model-dependent. However, the small differences observed in total couplings suggest that the effect of the CT states is slightly different in the dimers and the trimers. For example, AB and BC dimers of pentacene give γ total of 5.91 and 6.19 meV, respectively, and 4.50 and 3.38 meV when obtained from the corresponding trimer models. Thus, the size of the ensemble used does affect the γ total result. Similar changes in the total couplings are seen in the B,N-pentacene system. It can also be noticed that the total couplings obtained from trimer models, although related to the same dimer, can be noncoincident. For example, the γ for dimer AB in pentacene is 4.50 or 9.38 meV when obtained from ABC or ABD trimer models, respectively. Corresponding values for the B,N-pentacene system are 3.94 and 9.78 meV. This fact again brings up that the CT-state dressing acts differently on the same coupling parameter when the model changes. The major difference between dimers and trimers is that each singlet exciton and double triplet can interact with six CT states in the trimer, while there are only two CT states in the dimer.

Among the total couplings in pentacene, the largest γ = 9.38 meV (SF coupling), obtained for the ABD trimer, implies

https://doi.org/10.1021/acs.jpcc.4c08656
J. Phys. Chem. C 2025, 129, 4290−4302

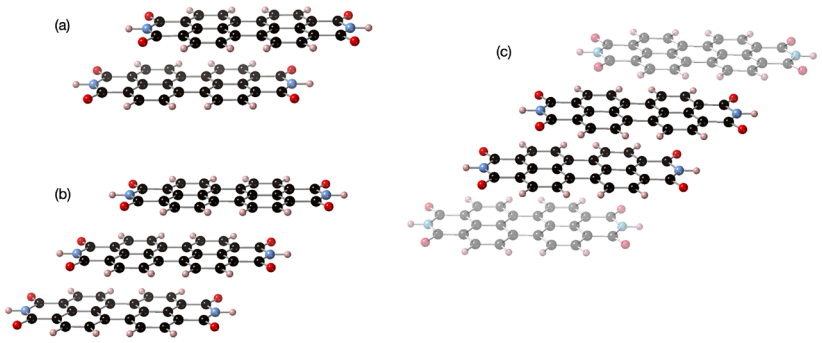

Figure 4. Perylenediimide models: dimer (a), trimer (b) and embedded dimer (c). Black spheres represent carbon atoms, light blue is nitrogen, red is oxygen and white is hydrogen. Shaded PDI molecules in (c) are represented as a frozen electronic density (see text).

Table 2. Direct and Total SF Electronic Couplings γ (in meV) for Dimers and Trimers of Crystalline Pentacene

	dimer				trimer	
	γ direct	γ total			γ direct	γ total
AB	1.61	5.91	ABC	AB	1.61	4.50
BC	0.42	6.19		BC	0.42	3.38
BD	1.59	5.93	ABD	AB = BD	1.66	9.38
AE = EF	0.13	0.40	AEF	AE = EF	0.13	0.59

Table 3. Direct and Total SF Electronic Couplings γ (in meV) for Dimers and Trimers of the B,N-Pentacene Doped Crystal[a,b]

	dimer				trimer	
	γ direct	γ total			γ direct	γ total
A<u>B</u>	0.65	8.48	A<u>B</u>C	A<u>B</u>	0.68	3.94
<u>B</u>C	2.38	1.73		<u>B</u>C	2.42	2.42
			A<u>B</u>D	A<u>B</u>	0.61	9.78
<u>B</u>D	3.64	33.18		<u>B</u>D	3.69	27.90
AE = EF	0.26	1.03	AEF	AE = EF	0.35	1.05

[a]Underlined labels correspond to pentacene units. [b]SF processes involving S_1 on the pentacene unit only.

nonparallel neighboring units (AB and BD). On the other hand, parallel units (AE) present the smallest SF couplings as anticipated above, showing the dependence of this phenomenon on geometrical characteristics. The B,N-pentacene system presents similar properties, with total values of the same order as pentacene. This system contains a pentacene unit (B, underlined in Table 3) and B,N-pentacene (all other units), see Figure 2. Because of the relative energies of the S_1 state in either unit type compared to the T_1T_1 state, the only excitations that meet the energy requirement for SF are those involving $S_0 \rightarrow S_1$ on pentacene units. Among the computed values, the nonparallel BD pair stands out with γ total = 33.18 and 27.90 meV, for the dimer and trimer models, respectively. Similar to the unsubstituted pentacene, the parallel AE dimer presents the smallest SF coupling.

The process of generating a separated triplet directly from a singlet exciton, $S_0S_1S_0 \rightarrow T_1S_0T_1$, computed for pentacene and B,N-pentacene gives negligible (<0.01) couplings in general. Only the parameters for ABC and ABD pentacene trimers get to 0.06 meV.

5.1.3. Indolonaphthyridine. The left part of Table 4 shows the total SF coupling in the regular stack of indolonaphthyridines, which turns out to be sizable (γ total = 12.14), yet not as large as in the PDI derivatives. As expected, the coupling

Table 4. Total SF Electronic Couplings (in meV) for a Regular and a Thermally Distorted Trimer of Indolonaphthyridines

	regular			distorted		
	$S_1S_0S_0$	$S_0S_1S_0$	$S_0S_0S_1$	$S_1S_0S_0$	$S_0S_1S_0$	$S_0S_0S_1$
$T_1T_1S_0$	12.58	11.68	0.03	38.92	17.89	3.85
$S_0T_1T_1$	0.03	11.68	12.58	2.66	20.19	1.42
$T_1S_0T_1$	0.04	<0.01	0.04	0.30	0.05	2.13

between the initial state with an excited state on one side of the stack and the double triplet state on the other is extremely small (~0.03 meV). The same is observed for the process in which the singlet exciton is directly converted into the separated triplet state ($S_1 \rightarrow T_1...T_1$), whose values are listed in the last row of the Table.

The thermally distorted stack shows a significant increase in the SF coupling when the S_1 state is on molecule A (see Figure 1) and the T_1T_1 state is formed on the AB unit: from 12.58 meV in the regular stack to 38.92 meV in the distorted one. An important factor in this increase is the fact that the two molecules are no longer parallel aligned along the *x*-axis as in the regular stack, but appear significantly rotated along the intermolecular axis (*z*-axis) in this snapshot of the MD simulation. This is in line with the observation of Masoomi and co-workers in PDI derivatives.[19] They observed larger SF couplings for the compounds where the molecules are not linearly stacked but rotated along *z* with respect to each other.

A second interesting feature of the distorted stack is the increase of the coupling between the singlet exciton on molecule C ($S_0S_0S_1$) and the triplet separated state $T_1S_0T_1$. Although not extremely large, a coupling of 2.13 meV is on the same order as the SF coupling found in the regular pentacene crystal. This makes the direct formation of the triplet separated state through singlet fission a realistic scenario. This increase is accompanied by a significant increase of the interaction of the singlet exciton localized on molecule C and the $T_1...T_1$ state with the $D^+S_0D^-$ and $D^-S_0D^+$ (see ESI, Table S2), confirming the suggestion of Wang et al.[20] that these *long-range* CT states with the electron and hole on non-neighboring molecules play an essential role in the direct formation of the $T_1...T_1$ state.

5.2. Triplet Separation. *5.2.1. Perylene Diimide.* As explained in the Introduction, once the T_1T_1 state is formed, the next step in the SF process involves its separation into two decoupled triplet states, therewith doubling the number of electron−hole pairs in the system. To study the separation and diffusion of the triplet states a minimal model containing three chromophores is indispensable. Here, we estimate these

https://doi.org/10.1021/acs.jpcc.4c08656
J. Phys. Chem. C 2025, 129, 4290−4302

parameters in a trimer model of PDI molecules in a stack (see Figure 4).

Table 5 reports the electronic couplings related to the triplet separation process, from $T_1T_1S_0$ or $S_0T_1T_1$ to $T_1S_0T_1$, and the ones related to the double triplet diffusion, i.e., from $T_1T_1S_0$ to $S_0T_1T_1$. Furthermore, it also lists the triplet separation energy ΔE, computed as the energy difference between the final state, where the triplet states are separated and the initial state, where the two triplets are located on nearest neighbor molecules. The separation of the dimer T_1T_1 state into two decoupled triplets is related to the T_1T_1 binding energy, E_b, which can be estimated as the energy difference between the dimer quintet state, $^5T_1T_1$, and the singlet T_1T_1 state as $E_b = E(^5T_1T_1) - E(^1T_1T_1)$. The energy of the quintet state of the dimer is considered in some model studies to give a reasonable estimate of the energy of two isolated triplet states.[9,33] The values of the binding energy in the dimer models, E_b, are also reported in Table 5 to allow comparison with the values obtained for the trimer. Positive values mean that triplet separation is not energetically favored. Comparing the triplet separation energies computed for the trimer and dimer models (see Table 5), shows that the quintet state approximation indeed leads to a fair estimate of this energy. The energy needed to separate the triplets varies depending on the PDI conformation. For the EP derivative, the triplet separation is not energetically favorable and in this conformation the adiabatic $T_1S_0T_1$ state turns out to be nearly pure, without any significant contribution from other MEBFs. Instead, triplet separation is more likely for the C3−I conformer. In this case, the $T_1T_1S_0$, $S_0T_1T_1$ and $T_1S_0T_1$ states are very close in energy and strongly mixed, thus enhancing the separation of the triplet states. Concerning the triplet separation energy, the PDI C7 derivative shows a comparable behavior to that observed for the C3−I while the C8 system behaves like the EP compound.

Table 5. Direct and Total Electronic Couplings (in meV) for Triplet Separation and Double Triplet Diffusion in Trimers of the PDI Derivatives[a]

	triplet separation		double triplet diffusion			
	direct	total	direct	total	ΔE	E_b dimer
EP	8.50	5.82	0.05	10.87	0.33	0.34
C3−I	1.73	1.32	<0.01	1.24	−0.03	0.11
C7	1.12	1.51	<0.01	1.37	0.03	0.10
C8	0.09	0.68	0.01	0.11	0.17	0.18

[a]Triplet separation energy (in eV) estimated for the trimer, ΔE, and the dimer, E_b (see text).

The values of the electronic couplings for the triplet separation are much larger for the EP conformation compared to the rest. The C8 derivative displays a small coupling for triplet separation, which will hinder the multiple exciton generation, despite the fact that the formation of the T_1T_1 state after photon absorption is favored by its large SF electronic coupling (see Table 1). For the C3−I and C7 derivatives, sizable values of the triplet separation coupling along with a small, or even negative, triplet separation energy, points to a favorable triplet separation.

The inclusion of both the charge transfer states and the effect of the electron correlation only has a moderate impact on the value of the couplings, as can be seen in Table 5 by comparing the direct and total couplings. The influence of these effects in the triplet separation coupling is much smaller than that found for the SF couplings (see Table 1), where the system changes from a $S_1S_0S_0$ to a $T_1T_1S_0$ state.

The electronic coupling derived from the $\langle T_1T_1S_0|\hat{H}|S_0T_1T_1\rangle$ matrix element gives an estimation of the probability of double triplet diffusion. The direct coupling for this process is virtually zero for all PDI conformations. However, inclusion of charge transfer effects has a drastic effect on these values, making this process feasible. Instead, incorporation of the electron correlation energy correction only slightly affects the couplings. Analysis of the wave functions of the $T_1T_1S_0$ and $S_0T_1T_1$ states, shows a strong mixing with the charge transfer states, as indicated by high weights of these MEBFs in the wave functions. For the EP conformer, the total electronic coupling for the double triplet diffusion is larger than the coupling for the triplet separation, fact that can be explained by the large triplet separation energy that hinders this process. In the other derivatives analyzed, the couplings for both processes are very similar and the triplet separation energies smaller, thus facilitating the separation of the triplet states.

The electronic couplings for the direct formation of the triplet separated state from the singlet excitonic state are in general small in all four PDI derivatives, see Table S3 of the ESI. The only exception is the C7 derivative, for which a coupling between the $S_1S_0S_0$ or $S_0S_0S_1$ and the $T_1S_0T_1$ state is 1.55 meV. This may facilitate the alternative route for triplet separation.

5.2.2. Pentacene and B,N-Pentacene. Triplet separation in the pentacene system (Table 6) presents moderate couplings in general, the largest ones computed for nonparallel neighboring fragments, that is, in trimers ABC, with 3.84 meV and ABD, with 1.26 meV. Instead, the AE → AF process is roughly 1 order of magnitude smaller (0.13 meV) since it involves parallel AEF units. It is noticeable that direct and total couplings are coincident and correspond to a negligible mixing of the CT states with any of the double triplets. The ΔE values listed, representing the energy increase from $T_1T_1S_0$ or $S_0T_1T_1$ to $T_1S_0T_1$, show nearly degenerate states. The similar direct and total couplings obtained for both pentacene and B,N-pentacene systems arise from the poor mixing of these double triplets with CT states. At variance with the pure pentacene crystal, the ΔE values are large and negative, except for the AE → AF process, since they involve the transfer of a T_1 state from pentacene to B,N-pentacene with an energy stabilization of ca. 0.6 eV. The T_1T_1 binding energies, E_b, are similar in pentacene

Table 6. Direct and Total Electronic Couplings (in meV) for Triplet Separation and Double Triplet Diffusion in Trimers of Crystalline Pentacene[a]

process	direct	total	ΔE	E_b dimer
	triplet separation			
AB → AC	3.85	3.84	0.01	0.02
BC → AC	1.25	1.24	0.02	0.03
AB → AD	1.25	1.26	0.03	0.02
AE → AF	0.13	0.13	0.003	0.01
	double triplet diffusion			
AB → BC	<0.01	0.09		
AB → BD	<0.01	0.22		
AE → EF	<0.01	<0.01		

[a]Triplet separation energy (in eV) estimated for the trimer, ΔE, and the dimer, E_b (see text).

https://doi.org/10.1021/acs.jpcc.4c08656
J. Phys. Chem. C 2025, 129, 4290−4302

and B,N-pentacene, and roughly half to one order magnitude smaller than the PDI values. This may indicate that triplet separation could be comparatively more favored in pentacene-based systems.

The electronic coupling for the double triplet diffusion systematically presents small values for pentacene and B,N-doped crystals, as shown in Tables 6 and 7. This phenomenon is, however, more affected by mixing with CT states, as can be deduced from the values associated with the pentacene AB → BD diffusion process, with direct and total couplings of <0.01 and 0.22 meV, respectively.

Table 7. Direct and Total Electronic Couplings (in meV) for Triplet Separation and Double Triplet Diffusion in Trimers of B,N-Pentacene[a]

process	direct	total	ΔE	E_b dimer
triplet separation				
AB → AC	3.92	3.92	−0.60	0.03
BC → AC	3.20	3.20	−0.54	0.02
AB → AD	1.43	1.44	−0.60	0.02
AE → AF	0.33	0.33	−0.02	0.03
double triplet diffusion				
AB → BC	<0.01	0.04		
AB → BD	<0.01	0.12		
AE → EF	<0.01	<0.01		

[a]Triplet separation energy (in eV) estimated for the trimer, ΔE, and the dimer, E_b (see text).

5.2.3. Indolonaphthyridine. The double triplet states ($T_1T_1S_0$ and $S_0T_1T_1$) of the regular stack of indolonaphthyridines are separated by less than 0.02 eV from the triplet separated state ($T_1S_0T_1$), and should be considered (quasi-)degenerate. Table 8 indicates that the coupling among these states is 3.13 meV, somewhat smaller than the SF coupling, but certainly not negligible. The combination of this near degeneracy and moderate electronic coupling leads to an adiabatic representation of these states that show strong mixing of the three MEBFs when only these three states are allowed to interact. However, after solving the full NOCI-F eigenvalue problem, this mixing disappears and the triplet separated state only contributes significantly to one of the NOCI-F eigenfunctions. The double triplet states interact strongly with the CT states and contribute to four wave functions in a significant manner (see Table S4)

Table 8. Total Triplet Separation and Double Triplet Diffusion Couplings (in meV) for a Regular and a Thermally Distorted Trimer of Indolonaphthyridines

	regular		distorted	
	$T_1T_1S_0$	$S_0T_1T_1$	$T_1T_1S_0$	$S_0T_1T_1$
$S_0T_1T_1$	0.11		0.04	
$T_1S_0T_1$	3.13	3.13	1.32	0.98

The binding energies of the double triplets in the distorted stack are −0.25 and −0.31 eV for the AB and the BC pairs, respectively. The coupling between these states is smaller than in the regular stack. This indicates that triplet separation is less likely in this distorted conformation than in the regular stack, counteracting the increase in the coupling between the singlet excitonic states and the double triplets. Table 8 also shows that the coupling for double triplet diffusion is weak, both in the regular and the distorted stacks.

Hence, the first step of singlet fission appears to be a likely event in the indolonaphthyridine stacks, but the next step of triplet separation may hinder the generation of two electron−hole pairs. A more extensive study is required to scan more snapshots of the MD trajectory to generalize this finding. It cannot be excluded beforehand that there are conformations for which triplet separation is more favorable than the ones studied here. Scanning a substantial number of conformations will most probably require application of a more approximate computational scheme such as the ab initio Frenkel Davydov approach, the Smith-Michl model or the method based on maximally localized fragment particle-hole densities.[15,38,61−64]

5.3. Singlet and Triplet Exciton Diffusion. *5.3.1. Perylene Diimide.* Table 9 collects the values of the coupling for the singlet diffusion process, where an S_1 state on one molecule diffuses to either a nearest neighbor (NN) or a next nearest neighbor (NNN) molecule. Equivalently, Table 10 gathers the couplings for the triplet diffusion process, where an isolated T_1 state moves to a nearest neighbor or a next nearest neighbor chromophore. The dimer model can only provide values of the coupling for the singlet and triplet diffusion between nearest neighbor molecules, using the $\langle S_0S_1|\hat{H}|S_1S_0\rangle$ and $\langle S_0T_1|\hat{H}|T_1S_0\rangle$ matrix elements, respectively, while the trimer model supplies information about the diffusion of the singlet and triplet excitons to nearest neighbor and next nearest neighbor molecules, $\langle S_1S_0S_0|\hat{H}|S_0S_1S_0\rangle$ and $\langle S_1S_0S_0|\hat{H}|S_0S_0S_1\rangle$ for the singlet exciton diffusion, and $\langle T_1S_0S_0|\hat{H}|S_0T_1S_0\rangle$ and $\langle T_1S_0S_0|\hat{H}|S_0S_0T_1\rangle$ for the triplet diffusion process.

Table 9. Direct and Total Electronic Couplings (in meV) for Singlet Exciton Diffusion in Dimer and Trimer Models of PDI

	dimer		trimer-NN[a]		trimer-NNN[b]	
	direct	total	direct	total	direct	total
EP	86.69	78.35	88.49	39.22	6.86	2.90
C3−I	93.52	65.61	95.10	72.29	8.86	9.48
C7	106.60	102.59	108.34	103.40	12.41	8.83
C8	106.13	72.34	107.92	80.06	9.18	4.11

[a]Nearest neighbor exciton diffusion. [b]Next nearest neighbor exciton diffusion.

Table 10. Direct and Total Electronic Couplings (in meV) for Triplet Exciton Diffusion in Dimer and Trimer Models of PDI

	dimer		trimer-NN[a]		trimer-NNN[b]	
	direct	total	direct	total	direct	total
EP	8.44	65.87	8.38	59.15	0.011	1.02
C3−I	1.73	6.21	1.70	5.75	0.002	0.11
C7	1.12	9.59	1.10	8.58	0.002	0.16
C8	0.10	3.10	0.08	2.48	0.009	0.45

[a]Nearest neighbor exciton diffusion. [b]Next nearest neighbor exciton diffusion.

Tables 9 and 10 allow a comparison of the electronic couplings for the exciton diffusion to a nearest neighbor molecule between the PDI dimer and trimer models (trimer-

https://doi.org/10.1021/acs.jpcc.4c08656
J. Phys. Chem. C 2025, 129, 4290−4302

NN in Tables 9 and 10). Results show a reasonable agreement in the couplings, both direct and total, between the two models for all the PDI derivatives studied, meaning that the dimer model already captures the essence of the mobility process to a nearest neighbor PDI molecule. Singlet exciton diffusion (see Table 9) to a nearest neighbor molecule displays large couplings, direct and total, for all PDI derivatives, pointing to a likely process and a tendency toward singlet exciton delocalization. Instead, diffusion of a singlet state to a next nearest neighbor molecule exhibits a smaller coupling, around 1 order of magnitude smaller, only contributing slightly to the delocalization of the singlet.

Triplet exciton diffusion (see Table 10) shows smaller couplings compared to the diffusion of the singlet exciton, roughly 1 order of magnitude smaller. Only the EP derivative displays a large value of the coupling. Contrary to the other derivatives studied, the EP conformer exhibits a minor displacement in the y direction (short molecular axis) between next neighbor molecules, such that the two nearest neighbor monomers are nearly on top of each other, which could promote the triplet mobility within different units. Again, as was found for the singlet exciton diffusion process, the diffusion of a triplet state to next nearest neighbor molecule is much less probable, as shown by the very small values of the $\langle T_1S_0S_0|\hat{H}|S_0S_0T_1\rangle$ coupling in Table 10.

Remarkably, the direct couplings for triplet exciton diffusion and triplet separation are nearly identical (cf. Tables 5 and 10). Given that the energy transfer involves the same molecules and the observation that the triplet binding energy is not very large, this coincidence of the couplings is not unexpected. The situation changes when the effect of dynamic correlation and the CT states are included and the two couplings are no longer (virtually) identical. This is caused by the different interactions of the triplet exciton and the double triplet with their respective CT states. In the first place, the relative energy of the isolated triplet exciton T_1 and the triplet coupled D^+D^-, D^-D^+ CT states is different from the energy difference between the singlet-coupled double triplet state T_1T_1 and the singlet CT states. Second, the Hamiltonian matrix elements between these states do not coincide. The large increase of the coupling for triplet exciton diffusion in the EP derivative from 8 to ∼60 meV is caused by an accidental degeneracy of the T_1 state with one of the CT states. This causes a strong mixing of these MEBFs, and consequently, a large total coupling of the triplets on neighboring molecules.

5.3.2. Pentacene and B,N-Pentacene. Couplings for the crystal arrangements of pentacene and B,N-pentacene are shown in Tables 11 and 12. First, the values of singlet exciton diffusion are notably smaller than those listed for the PDI models in Table 9, a difference originating in the diverse mutual fragment orientations. In Table 11, the AB, BC and BD dimers (nonparallel NN) present smaller couplings than the AE dimer (parallel NN). Direct couplings computed for dimer and trimer models coincide. However, differences between models appear after including the CT mixing and dynamical electron correlation energy. In trimers, more CT states can participate in dressing the singlet exciton states allowing for a different role, which not always leads to increasing the direct couplings. Two main factors govern enhancement or reduction of the singlet exciton diffusion couplings when considering the CT states and dynamic correlation corrections. Figure 5 shows three different cases of dimers to explain the interplay between both effects. The first case (pentacene AB) shows a coupling

Table 11. Direct and Total Electronic Couplings (in meV) for Singlet Exciton Diffusion in Dimer and Trimer Models of Crystalline Pentacene and B,N-Pentacene

		pentacene		B,N-pentacene	
dimer		direct	total	direct	total
AB		11.50	0.93	2.27	20.05
BC		15.49	12.72	0.15	21.94
BD		11.03	0.46	7.91	9.99
AE = EF		38.63	39.26	39.63	40.13
trimer		direct	total	direct	total
ABC	AB	11.62	1.80	3.24	16.30
	BC	20.06	6.31	1.84	11.36
	AC	7.81	7.68	15.78	16.49
ABD	AB	11.61	3.83	9.05	17.56
	BD	10.72	4.55	4.90	9.12
	AD	6.87	6.76	4.80	5.81
AEF	AE = EF	38.69	39.30	34.72	35.10
	AF	5.91	5.92	7.75	7.52

Table 12. Direct and Total Electronic Couplings (in meV) for Triplet Exciton Diffusion in Dimer and Trimer Models of Crystalline Pentacene and B,N-Pentacene

		pentacene		B,N-pentacene	
dimer		direct	total	direct	total
AB		1.26	4.41	3.18	6.42
BC		3.79	12.28	3.83	7.41
BD		1.26	4.43	1.42	3.78
AE		0.13	0.39	0.34	0.94
trimer		direct	total	direct	total
ABC	AB	1.26	4.37	3.19	6.15
	BC	3.84	12.27	3.88	7.50
	AC	<0.01	0.02	0.03	0.04
ABD	AB	1.25	3.96	3.18	6.60
	BD	1.25	3.96	1.41	4.02
	AD	<0.01	<0.01	<0.01	<0.01
AEF	AE	0.13	0.38	0.33	0.83
	EF	0.13	0.38		
	AF	<0.01	<0.01	<0.01	<0.01

that decreases when CT states dress the S_1S_0 and S_0S_1 states. The D^+D^-, D^-D^+ coefficients are large in the dressed singlet exciton MEBFs, which should in principle lead to a considerable increase of the coupling. However, the mixing is accompanied by a considerable increase of the separation of the excited singlet states. The combination of these two effects results in a slight decrease of the coupling between the two singlet excitons. When the dynamic correlation energy correction is added, the gap between the CT states and the singlet excitons becomes much larger and the coupling decreases to 0.93 meV due to a smaller weight of CT states. The Pentacene AE case presents no change of the coupling along the series. The coupling of ca. 39 meV does not originate in the mixing with CT states, but in the near degeneracy of the S_1S_0 and S_0S_1 states. In fact, the coupling obtained with CT-enhanced functions is practically the same. Finally, a marked increase in the coupling is observed for B,N-pentacene AB. In this case, the direct coupling of 2.27 meV is the smallest in the series due to a large energy separation between S_1S_0 and S_0S_1. By mixing these with CT states a large increase in the coupling is obtained, based on sizable D^+D^- and D^-D^+ coefficients. Including the dynamical electron correlation to the NOCI

https://doi.org/10.1021/acs.jpcc.4c08656
J. Phys. Chem. C 2025, 129, 4290−4302

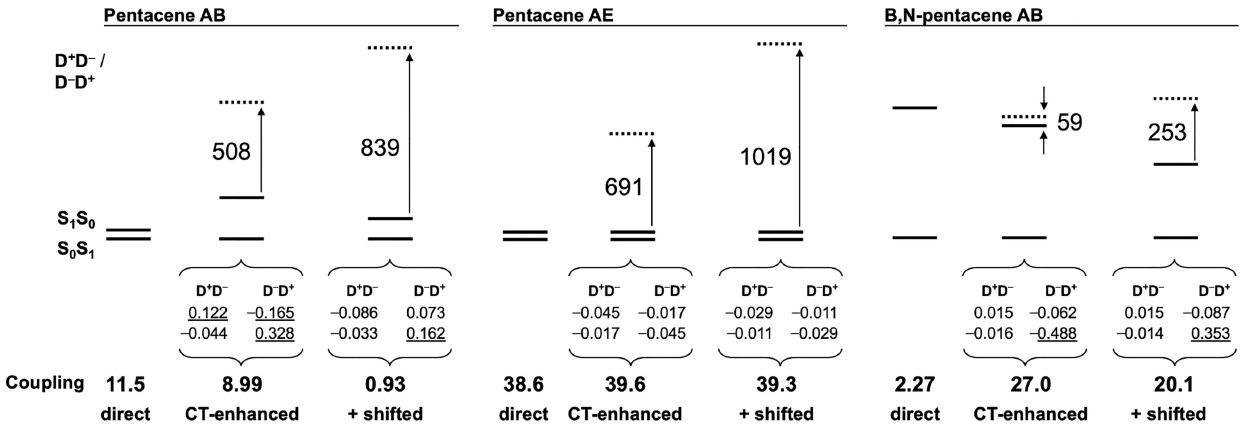

Figure 5. State energy sequence (in meV, no to scale) relevant for the singlet exciton diffusion process. The direct, CT-enhanced and total (+shifted) coupling parameters (in meV) are shown. When the CT dressing is included, the major contributions are shown underlined.

energies leads again to an increase of the energy separation between the singlet exciton and CT states, which lowers the degree of mixing and a decrease in the total coupling to 20.1 meV.

5.3.3. Indolonaphthyridine. The singlet and triplet exciton diffusion couplings listed in Tables 13 and 14 roughly follow the same tendency as the ones observed for the PDI trimers. The coupling of singlets on nearest neighbors is strong upon neighbors in the regular stack and persists to some extent when looking at the next nearest neighbors. Distortions significantly reduce the coupling and, combined with the fact that the energies of the local excited singlets on the three fragments are no longer the same, this leads to a drastic decrease of the delocalization of the singlet exciton. The isolated triplet exciton is only weakly coupled to its neighbors, both in the regular and the distorted stacks, indicating a slow diffusion process after the formation of the $T_1...T_1$ state.

Table 13. Total Singlet Exciton Diffusion Couplings (in meV) for a Regular and a Thermally Distorted Trimer of Indolonaphthyridines

	regular		distorted	
	$S_1S_0S_0$	$S_0S_1S_0$	$S_1S_0S_0$	$S_0S_1S_0$
$S_0S_1S_0$	78.02		46.97	
$S_0S_0S_1$	11.65	78.02	2.04	12.34

Table 14. Total Triplet Exciton Diffusion Couplings (in meV) for a Regular and a Thermally Distorted Trimer of Indolonaphthyridines

	regular		distorted	
	$T_1S_0S_0$	$S_0T_1S_0$	$T_1S_0S_0$	$S_0T_1S_0$
$S_0T_1S_0$	0.70		0.85	
$S_0S_0T_1$	<0.01	0.70	0.01	0.53

6. CONCLUSIONS

Singlet fission intermolecular electronic couplings, singlet and triplet exciton diffusion and triplet separation processes have been analyzed by Non-Orthogonal Configuration Interaction with Fragments (NOCI-F). Four different compounds were studied, of which three (PDI, pentacene and indolonaphthyridine) are known to show singlet fission, while BN-pentacene has been proposed as an interesting alternative for unsubstituted pentacene.

The comparison of ensembles with two or three molecules shows that the direct couplings for singlet fission, and singlet and triplet diffusion are the same in both models. In most cases this resemblance is maintained in the total couplings (adding the CT and dynamic correlation effects), but the fact that more CT states can be defined in the trimer results in discrepancies between dimer and trimer results. The differences are, however, never large enough to qualitatively change the conclusions that can be drawn from a (computationally less expensive) dimer calculation.

To study the fate of the intermediate state of the singlet fission process (the singlet-coupled double triplet), dimer models are no longer sufficient. Triplet separation and double triplet diffusion were studied in ensembles with three molecules. The binding energy of the double triplet state T_1T_1 varies from almost zero in the regular indolonaphthyridine stack to 0.85 eV along the diagonal of the unit cell of pentacene. The couplings between the T_1T_1 and $T_1...T_1$ states are in general smaller than the singlet fission couplings and lie in all cases in the interval running from 1 to 10 meV. This implies that triplet separation is presumably a comparatively slow process and efficiency losses can be expected at this stage of the generation of the four charge carriers.

An alternative scenario for the generation of the $T_1...T_1$ state has been studied, namely directly from the singlet excitonic state. In the regular structures, the electronic coupling between S_1 and $T_1...T_1$ is extremely small, even when dynamic correlation and CT effects are accounted for. Only in the distorted stack of indolonaphthyridines we observed a non-negligible coupling. This possibility must be further explored by scanning other snapshots of the MD trajectory, but thermally distorted conformations tend to reduce the delocalization and the diffusion of the excitonic states.

The electronic couplings for singlet diffusion are among the largest couplings studied here, especially among molecules that are parallel to each other. Thermal distortions of the structure and nonparallel alignments (for example along the diagonal of the pentacene unit cell) reduce this coupling. Although sharing the same orbital occupation, the coupling for triplet diffusion is in general much smaller than the coupling for singlet diffusion. The frontier molecular orbital model of Smith and Michl provides a rationale for this difference.[22] The singlet exciton coupling is proportional to the two-electron integral $(ab|cd)$

https://doi.org/10.1021/acs.jpcc.4c08656
J. Phys. Chem. C 2025, 129, 4290−4302

with *ab* on center 1 and *cd* on center 2. In contrast, the triplet exciton coupling is proportional in this approximate model to (*ac*|*bd*), which is much smaller since *ac* and *bd* involve orbitals on different centers.

■ ASSOCIATED CONTENT

Supporting Information

The Supporting Information is available free of charge at https://pubs.acs.org/doi/10.1021/acs.jpcc.4c08656.

Displacements of the molecules in the four PDI stacks; direct and total couplings for the S_1 to T_1...T_1 process in PDI; singlet NOCI-F wave functions of the regular indolonaphthyridine stack; electronic coupling between the S_1 and T_1T_1 and the CT states in the regular and distorted indolonaphthyridine stacks (PDF)

■ AUTHOR INFORMATION

Corresponding Author

C. Sousa − *Departament de Ciència de Materials i Química Física and Institut de Química Teòrica i Computacional, Universitat de Barcelona, 08028 Barcelona, Spain;* orcid.org/0000-0002-1915-1111; Email: c.sousa@ub.edu

Authors

X. López − *Departament de Química Física i Inorgànica, Universitat Rovira i Virgili, 43007 Tarragona, Spain;* orcid.org/0000-0003-0322-6796

X. Dong − *National Center for Computational Sciences, Oak Ridge National Laboratory, Oak Ridge, Tennessee 37831-6373, United States*

R. Broer − *Zernike Institute for Advanced Materials, University of Groningen, 9747 AG Groningen, The Netherlands;* orcid.org/0000-0002-5437-9509

T. P. Straatsma − *National Center for Computational Sciences, Oak Ridge National Laboratory, Oak Ridge, Tennessee 37831-6373, United States; Department of Chemistry and Biochemistry, University of Alabama, Tuscaloosa, Alabama 35487-0336, United States;* orcid.org/0000-0001-5150-643X

C. de Graaf − *Departament de Química Física i Inorgànica, Universitat Rovira i Virgili, 43007 Tarragona, Spain; ICREA, 08010 Barcelona, Spain;* orcid.org/0000-0001-8114-6658

Complete contact information is available at: https://pubs.acs.org/10.1021/acs.jpcc.4c08656

Notes

The authors declare no competing financial interest.

This manuscript has been authored in part by UT-Battelle, LLC, under contract DE-AC05−00OR22725 with the US Department of Energy (DOE). The US government retains and the publisher, by accepting the article for publication, acknowledges that the US govern-ment retains a nonexclusive, paid-up, irrevocable, worldwide license to publish or reproduce the published form of this manuscript, or allow others to do so, for US government purposes. DOE will provide public access to these results of federally sponsored research in accordance with the DOE Public Access Plan (http://energy.gov/downloads/doe-public-access-plan).

■ ACKNOWLEDGMENTS

Financial support was provided by the ministry of science and innovation of the Spanish administration through the projects PID2021-126076NB-I00, PID2020-113187GB-I00, and Maria de Maetzu CEX2021-001202-M and by the Generalitat de Catalunya through the projects 2021SGR00079 and 2021SGR00110. This work used resources of the Oak Ridge Leadership Computing Facility (OLCF) at the Oak Ridge National Laboratory, which is supported by the Office of Science of the U.S. Department of Energy (DOE) under Contract DE-AC05-00OR22725 through the INCITE Project CHM154 and SummitPLUS Project CHM198. Part of the calculations were performed on Leonardo@CINECA (Italy) within the EuroHPC-JU programme.

■ REFERENCES

(1) Zeng, T.; Goel, P. Design of Small Intramolecular Singlet Fission Chromophores: An Azaborine Candidate and General Small Size Effects. *J. Phys. Chem. Lett.* **2016**, *7*, 1351−1358.

(2) Japahuge, A.; Zeng, T. Theoretical Studies of Singlet Fission: Searching for Materials and Exploring Mechanisms. *ChemPlusChem.* **2018**, *83*, 146−182.

(3) Pradhan, E.; Bentley, J. N.; Caputo, C. B.; Zeng, T. Designs of singlet fission chromophores with a diazadiborinine framework. *ChemPhotoChem.* **2020**, *4*, 5279−5287.

(4) Fallon, K. J.; Bronstein, H. Indolonaphthyridine: A Versatile Chromophore for Organic Electronics Inspired by Natural Indigo Dye. *Acc. Chem. Res.* **2021**, *54*, 182−193.

(5) Zeng, T.; Ananth, N.; Hoffmann, R. Seeking Small Molecules for Singlet Fission: A Heteroatom Substitution Strategy. *J. Am. Chem. Soc.* **2014**, *136*, 12638−12647.

(6) Ito, S.; Nagami, T.; Nakano, M. Molecular design for efficient singlet fission. *J. Photochem. Photobiol. C-Photochem. Rev.* **2018**, *34*, 85−120.

(7) Fallon, K. J.; Budden, P.; Salvadori, E.; Ganose, A. M.; Savory, C. N.; Eyre, L.; Dowland, S.; Ai, Q.; Goodlett, S.; Risko, C.; et al. Exploiting Excited-State Aromaticity To Design Highly Stable Singlet Fission Materials. *J. Am. Chem. Soc.* **2019**, *141*, 13867−13876.

(8) El Bakouri, O.; Smith, J. R.; Ottoson, H. Strategies for Design of Potential Singlet Fission Chromophores Utilizing a Combination of Ground-State and Excited-State Aromaticity Rules. *J. Am. Chem. Soc.* **2020**, *142*, 5602−5617.

(9) Casanova, D. Theoretical Modeling of Singlet Fission. *Chem. Rev.* **2018**, *118*, 7164−7207.

(10) Zaykov, A.; Felkel, P.; Buchanan, E. A.; Jovamovic, M.; Havenith, R. W. A.; Kathir, R. K.; Broer, R.; Havlas, Z.; Michl, J. Singlet Fission Rate: Optimized Packing of a Molecular Pair. Ethylene as a Model. *J. Am. Chem. Soc.* **2019**, *141*, 17729−17743.

(11) Greiner, J. E.; Singh, A.; Röhr, M. I. S. Functionality optimization for effective singlet fission coupling screening in the full-dimensional molecular and intermolecular coordinate space. *Phys. Chem. Chem. Phys.* **2024**, *26*, 19257−19265.

(12) Miyata, K.; Conrad-Burton, F. S.; Geyer, F. L.; Zhu, X.-Y. Triplet Pair States in Singlet Fission. *Chem. Rev.* **2019**, *119*, 4261−4292.

(13) Casillas, R.; Papadopoulos, I.; Ullrich, T.; Thiel, D.; Kunzmann, A.; Guldi, D. M. Molecular insights and concepts to engineer singlet fission energy conversion devices. *Energy Environ. Sci.* **2020**, *13*, 2741−2804.

(14) Carrod, A. J.; Gray, V.; Börjesson, K. Recent advances in triplet−triplet annihilation upconversion and singlet fission, towards solar energy applications. *Energy Environ. Sci.* **2022**, *15*, 4982.

(15) Singh, A.; Röhr, M. I. S. Configuration Interaction in Frontier Molecular Orbital Basis for Screening the Spin-Correlated, Spatially Separated Triplet Pair State ^{1}(T···T) Formation. *J. Chem. Theory Comput.* **2024**, *20*, 8624−8633.

(16) Yong, C. K.; Musser, A. J.; Bayliss, S. L.; Lukman, S.; Tamura, H.; Bubnova, O.; Hallani, R. K.; Meneau, A.; Resel, R.; Maruyama, M.; et al. The entangled triplet pair state in acene and heteroacene materials. *Nat. Commun.* **2017**, *8*, No. 15953.
(17) Bossanyi, D. G.; Matthiesen, M.; Wang, S.; Smith, J. A.; Kilbride, R.; Shipp, J. D.; Chekulaev, D.; Holland, E.; Anthony, J. E.; Zaumseil, J.; et al. Emissive spin-0 triplet-pairs are a direct product of triplet−triplet annihilation in pentacene single crystals and anthradithiophene films. *Nat. Chem.* **2021**, *13*, 163−171.
(18) Purdy, M.; Budden, P.; Fallon, K.; Gannett, C. N.; Abruña, H. D.; Zeng, W.; Friend, R.; Musser, A. J.; Bronstein, H. Re-Thinking Dimer Design Principles with Indolonaphthyridine Intramolecular Singlet Fission. *Chem.—Eur. J.* **2023**, *29*, No. e202301547.
(19) Masoomi-Godarzi, S.; Hall, C. R.; Zhang, B.; Gregory, M. A.; White, J. M.; Wong, W. W. H.; Ghiggino, K. P.; Smith, T. A.; Jones, D. J. Competitive Triplet Formation and Recombination in Crystalline Films of Perylenediimide Derivatives: Implications for Singlet Fission. *J. Phys. Chem. C* **2020**, *124*, 11574−11585.
(20) Wang, Z.; Liu, H.; Xie, X.; Zhang, C.; Wang, R.; Chen, L.; Xu, Y.; Ma, H.; Fang, W.; Yao, Y.; et al. Free-triplet generation with improved efficiency in tetracene oligomers through spatially separated triplet pair states. *Nat. Chem.* **2021**, *13*, 559−567.
(21) Refaely-Abramson, S.; da Jornada, F. H.; Louie, S. G.; Neaton, J. B. Origins of Singlet Fission in Solid Pentacene from an ab initio Green's Function Approach. *Phys. Rev. Lett.* **2017**, *119*, No. 267401.
(22) Sánchez-Mansilla, A.; Stan, I. O.; Broer, R.; de Graaf, C. Exciton delocalisation and triplet diffusion in singlet fission materials: A many-electron tight-binding and non-orthogonal CI study. *J. Phys. Chem. C* **2025**, *129*, 2797.
(23) Sousa, C.; Sánchez-Mansilla, A.; Broer, R.; Straatsma, T. P.; de Graaf, C. A Nonorthogonal Configuration Interaction Approach to Singlet Fission in Perylenediimide Compounds. *J. Phys. Chem. A* **2023**, *127*, 9944−9958.
(24) Pinheiro, M., Jr; Machado, F. B. C.; Plasser, F.; Aquino, A. J. A.; Lischka, H. A systematic analysis of excitonic properties to seek optimal singlet fission: the BN-substitution patterns in tetracene. *J. Mater. Chem. C* **2020**, *8*, 7793−7804.
(25) Singh, A.; Humeniuk, A.; Röhr, M. I. S. Energetics and optimal molecular packing for singlet fission in BN-doped perylenes: electronic adiabatic state basis screening. *Phys. Chem. Chem. Phys.* **2021**, *23*, 16525−16536.
(26) López, X.; Straatsma, T. P.; Sánchez-Mansilla, A.; de Graaf, C. Non-orthogonal Configuration Interaction Study on the Effect of Thermal Distortions on the Singlet Fission Process in Photoexcited Pure and B,N-Doped Pentacene Crystals. *J. Phys. Chem. C* **2023**, *127*, 16249−16258.
(27) Sánchez-Mansilla, A.; Sousa, C.; Kathir, R. K.; Broer, R.; Straatsma, T. P.; de Graaf, C. On the role of dynamic electron correlation in non-orthogonal configuration interaction with fragments. *Phys. Chem. Chem. Phys.* **2022**, *24*, 11931−11944.
(28) Straatsma, T. P.; Broer, R.; Faraji, S.; Havenith, R. W. A.; Suarez, L. E. A.; Kathir, R. K.; Wibowo, M.; de Graaf, C. GronOR: Massively parallel and GPU-accelerated non-orthogonal configuration interaction for large molecular systems. *J. Chem. Phys.* **2020**, *152*, No. 064111.
(29) Straatsma, T. P.; Broer, R.; Sánchez-Mansilla, R. A.; Sousa, C.; de Graaf, C. GronOR: Scalable and Accelerated Nonorthogonal Configuration Interaction for Molecular Fragment Wave Functions. *J. Chem. Theory Comput.* **2022**, *18*, 3549−3565.
(30) Kathir, R. K.; de Graaf, C.; Broer, R.; Havenith, R. W. A. Reduced Common Molecular Orbital Basis for Nonorthogonal Configuration Interaction. *J. Chem. Theory Comput.* **2020**, *16*, 2941−2951.
(31) Broer, R.; Nieuwpoort, W. C. Broken orbital symmetry and the description of valence hole states in the tetrahedral $[CrO_4]^{2-}$ anion. *Theor. Chim. Acta* **1988**, *73*, 405−418.
(32) de Graaf, C.; Broer, R.; Straatsma, T. P. In *Reference Module in Chemistry, Molecular Sciences and Chemical Engineering*; Shaik, S.; Hiberty, P., Eds.; Elsevier, 2023.
(33) Farag, M. H.; Krylov, A. I. Singlet Fission in Perylenediimide Dimers. *J. Phys. Chem. C* **2018**, *122*, 25753−25763.
(34) Zeng, T.; Mellerup, S. K.; Yang, D.; Wang, X.; Wang, S.; Stamplecoskie, K. Identifying (BN)2-pyrenes as a New Class of Singlet Fission Chromophores: Significance of Azaborine Substitution. *J. Phys. Chem. Lett.* **2018**, *9*, 2919−2927.
(35) Walia, R.; Yang, J. Exploring optimal multimode vibronic pathways in singlet fission of azaborine analogues of perylene. *Photochem. Photobiol. Sci.* **2022**, *21*, 1689−1700.
(36) Zhuang, F.-D.; Sun, Z.-H.; Yao, Z.-F.; Chen, Q.-R.; Huang, Z.; Yang, J.-H.; Wang, J.; Pei, J. BN-Embedded Tetrabenzopentacene: A Pentacene Derivative with Improved Stability. *Angew. Chem., Int. Ed.* **2019**, *58*, 10708−10712.
(37) Aguilar Suarez, L. E.; Menger, M. F. S. J.; Faraji, S. Singlet fission in tetracene: an excited state analysis. *Mol. Phys.* **2020**, *118*, No. e1769870.
(38) López, X.; Sánchez-Mansilla, A.; Sousa, C.; Straatsma, T. P.; Broer, R.; de Graaf, C. Comparison of Computational Strategies for the Calculation of the Electronic Coupling in Intermolecular Energy and Electron Transport Processes. *J. Phys. Chem. A* **2023**, *127*, 10717−10731.
(39) Becke, A. D. Density-functional exchange-energy approximation with correct asymptotic behavior. *Phys. Rev. A* **1988**, *38*, 3098−3100.
(40) Perdew, J. P. Accurate and simple density functional for the electronic exchange energy: Generalized gradient approximation. *Phys. Rev. B* **1986**, *33*, 8800.
(41) Grimme, S.; Antony, J.; Ehrlich, S.; Krieg, H. A consistent and accurate ab initio parametrization of density functional dispersion correction (DFT-D) for the 94 elements H-Pu. *J. Chem. Phys.* **2010**, *132*, 154104.
(42) Weigend, F.; Ahlrichs, R. Balanced basis sets of split valence, triple zeta valence and quadruple zeta valence quality for H to Rn: Design and assessment of accuracy. *Phys. Chem. Chem. Phys.* **2005**, *7*, 3297−3305.
(43) Neese, F.; Wennmohs, F.; Becker, U.; Riplinger, C. The ORCA quantum chemistry program package. *J. Chem. Phys.* **2020**, *152*, 224108.
(44) Kresse, G.; Hafner, J. Ab Initio Molecular Dynamics for Liquid Metals. *Phys. Rev. B* **1993**, *47*, 558−561.
(45) Kresse, G.; Hafner, J. Ab initio molecular-dynamics simulation of the liquid-metal —amorphous-semiconductor transition in germanium. *Phys. Rev. B* **1994**, *49*, 14251−14269.
(46) Kresse, G.; Furthmüller, J. Efficient iterative schemes for ab initio total-energy calculations using a plane-wave basis set. *Phys. Rev. B* **1996**, *54*, 11169−11186.
(47) Kresse, G.; Furthmüller, J. Efficiency of ab-initio total energy calculations for metals and semiconductors using a plane-wave basis set. *Comput. Mater. Sci.* **1996**, *6*, 15−50.
(48) Perdew, J. P.; Burke, K.; Ernzerhof, M. Generalized Gradient Approximation Made Simple. *Phys. Rev. Lett.* **1996**, *77*, 3865.
(49) Valiev, M.; Bylaska, E.; Govind, N.; Kowalski, K.; Straatsma, T. P.; van Dam, H.; Wang, D.; Nieplocha, J.; Apra, E.; Windus, T.; et al. NWChem: a comprehensive and scalable open-source solution for large scale molecular simulations. *Comput. Phys. Commun.* **2010**, *181*, 1477.
(50) Becke, A. D. Density-functional thermochemistry. III. The role of exact exchange. *J. Chem. Phys.* **1993**, *98*, 5648−5652.
(51) Lee, C.; Yang, W.; Parr, R. G. Development of the Colle-Salvetti correlation-energy formula into a functional of the electron density. *Phys. Rev. B* **1988**, *37*, 785.
(52) Hess, B.; Kutzner, C.; van der Spoel, D.; Lindahl, E. GROMACS 4: Algorithms for highly efficient, load-balanced, and scalable molecular simulation. *J. Chem. Theory Comput.* **2008**, *4*, 435−447.
(53) Wang, J.; Cieplak, P.; Kollman, P. A. ow well does a restrained electrostatic potential (RESP) model perform in calculating conformational energies of organic and biological molecules? *J. Comput. Chem.* **2000**, *21*, 1049−1071.

https://doi.org/10.1021/acs.jpcc.4c08656
J. Phys. Chem. C 2025, 129, 4290−4302

(54) Case, D. A.; Cheatham, T. E.; Darden, T.; Gohlke, H.; Luo, R.; Merz, K. M.; Onufriev, A.; Simmerling, C.; Wang, B.; Woods, R. The AMBER Biomolecular Simulation Programs. *J. Comput. Chem.* **2005**, *26*, 1668−1688.
(55) Bussi, G.; Donadio, D.; Parrinello, M. Canonical sampling through velocity rescaling. *J. Chem. Phys.* **2007**, *126*, No. 014101.
(56) Angeli, C.; Cimiraglia, R.; Evangelisti, S.; Leininger, T.; Malrieu, J.-P. Introduction of n-electron valence states for multi-reference perturbation theory. *J. Chem. Phys.* **2001**, *114*, 10252−10264.
(57) Freitag, L.; Knecht, S.; Angeli, C.; Reiher, M. Multireference Perturbation Theory with Cholesky Decomposition for the Density Matrix Renormalization Group. *J. Chem. Theory Comput.* **2017**, *13*, 451−459.
(58) Aquilante, F.; Autschbach, J.; Baiardi, A.; Battaglia, S.; Borin, V. A.; Chibotaru, L. F.; Conti, I.; De Vico, L.; Delcey, M.; Fdez. Galvén, I.; Ferré, N.; Freitag, L.; Garavelli, M.; Gong, X.; Knecht, S.; Larsson, E. D.; Lindh, R.; Lundberg, M.; Malmqvist, P. Å.; Nenov, A.; Norell, J.; Odelius, M.; Olivucci, M.; Pedersen, T. B.; Pedraza-Gonzélez, L.; Phung, Q. M.; Pierloot, K.; Reiher, M.; Schapiro, I.; Segarra-Martí, J.; Segatta, F.; Seijo, L.; Sen, S.; Sergentu, D. C.; Stein, C. J.; Ungur, L.; Vacher, M.; Valentini, A.; Veryazov, V.; et al. Modern quantum chemistry with [Open]Molcas. *J. Chem. Phys.* **2020**, *152*, 214117.
(59) Li Manni, G.; Galván, I. F.; Alavi, A.; Aleotti, F.; Aquilante, F.; Autschbach, J.; Avagliano, D.; Baiardi, A.; Bao, J. J.; Battaglia, S.; et al. The OpenMolcas Web: A Community-Driven Approach to Advancing Computational Chemistry. *J. Chem. Theory Comput.* **2023**, *19*, 6933−6991.
(60) Roos, B. O.; Lindh, R.; Malmqvist, P.-Å.; Veryazov, V.; Widmark, P.-O. Main Group Atoms and Dimers Studied with a New Relativistic ANO Basis Set. *J. Phys. Chem. A* **2004**, *108*, 2851−2858.
(61) Smith, M. B.; Michl, J. Singlet Fission. *Chem. Rev.* **2010**, *110*, 6891−6936.
(62) Morrison, A. F.; You, Z.-Q.; Herbert, J. M. Ab Initio Implementation of the Frenkel-Davydov Exciton Model: A Naturally Parallelizable Approach to Computing Collective Excitations in Crystals and Aggregates. *J. Chem. Theory Comput.* **2014**, *10*, 5366−5376.
(63) Smith, M. B.; Michl, J. Recent Advances in Singlet Fission. *Annu. Rev. Phys. Chem.* **2013**, *64*, 361−386.
(64) Wang, Y.-C.; Feng, S.; Kong, Y.; Huang, X.; Liang, W.-Z.; Zhao, Y. Electronic Couplings for Singlet Fission Processes Based on the Fragment Particle-Hole Densities. *J. Chem. Theory Comput.* **2023**, *19*, 3900−3914.

https://doi.org/10.1021/acs.jpcc.4c08656
J. Phys. Chem. C 2025, 129, 4290−4302